Advances in Industrial and Manufacturing Engineering 12 (2026) 100180

Contents lists available at ScienceDirect

Advances in Industrial and Manufacturing Engineering

journal homepage: www.sciencedirect.com/journal/advances-in-industrial-and-manufacturing-engineering

Joining-by-hydroforming of aluminum and poly(ether ether ketone) – A model experiment

Florian Weber [a,*], Ulrich A. Handge [b], Tanmoy Rakshit [a], Hamed Dardaei Joghan [a], Marlon Hahn [a], Yannis P. Korkolis [a], A. Erman Tekkaya [a]

[a] Institute of Forming Technology and Lightweight Components (IUL), TU Dortmund University, 44227, Dortmund, Germany
[b] Chair of Plastics Technology (LKT), TU Dortmund University, 44227, Dortmund, Germany

ARTICLE INFO

Keywords:
Joining
Tube
Aluminum
poly(ether ether ketone)
Stress relaxation

ABSTRACT

Joining-by-hydroforming is a process in which components are joined through expansion under internal pressure. Depending on the required fluid pressure and application rate, this process can be technically demanding and challenging to implement on industrial equipment. To address this, a simplified experimental setup was developed to investigate the fundamental joining mechanisms. In this setup, aluminum 6061-T6 (AA6061-T6) and poly(ether ether ketone) (PEEK) rings are force-fitted using a conical punch and segmented conical expansion elements, enabling controlled radial expansion. The resulting assemblies are subsequently separated in a dedicated push-out test. Experimental results show that the required separation force increases with rising elastic strain in the polymer, attributable to an increase in contact pressure according to Coulomb's friction law. This effect diminishes once plastic deformation of the thermoplastic initiates. Furthermore, stress relaxation in PEEK causes a time-dependent decrease in joint strength, reaching a quasi-equilibrium after approximately 10^4 s, as confirmed by relaxation experiments on PEEK coupons. To analyze thermal effects, the entire ring assembly is preheated to defined temperatures in a laboratory furnace. An inverse correlation between joining temperature and joint strength is observed, consistent with the trend identified in the dynamic-mechanical-thermal analysis (DMTA) of PEEK.

The proposed experimental method enables rapid identification of the most influential parameters for joining-by-hydroforming, without requiring dedicated hydroforming equipment or production machine time.

1. Introduction

The mechanical performance of a component is significantly influenced by its structural integrity, often leading to the conclusion that a monolithic structure is preferable. However, these monolithic structures are impractical due to the spatial limitations inherent in most manufacturing processes (Amancio-Filho and dos Santos, 2009). This motivates the application of material lightweighting design strategies, where a material is substituted with an alternative that offers superior specific properties (Hahn et al., 2019), as well as hybridization through the integration of dissimilar materials within a single component. In this context, joining of metals and polymers appears particularly promising, as such hybrid joints can combine the strength and ductility of metals with the low density and high chemical resistance of polymers (Balle et al., 2009). This study focuses on the joining of aluminum 6061-T6 (AA6061-T6) and poly(ether ether ketone) (PEEK).

The Aluminum alloy 6061-T6 is widely used in the aerospace and transportation industries due to its high strength-to-weight ratio and excellent corrosion resistance (Agarwal et al., 2003). Roy et al. (2022) examined its mechanical behavior through uniaxial tensile tests at temperatures up to 500 °C and found that up to approximately 150 °C, the yield strength, ultimate tensile strength, and Young's modulus showed only minor reductions compared to room temperature (RT). In contrast, elongation at break and uniform elongation remained nearly temperature-independent in that same range. Regarding strain-rate sensitivity, Scapin and Manes (2018) conducted both quasi-static uniaxial tensile tests and dynamic Split-Hopkinson bar tests. They observed that the material's mechanical response was largely unaffected in the range of 10^{-3} to 10^{-1} s^{-1}, while higher strain rates between 10^3 and 10^4 s^{-1} led to a noticeable increase in strength.

The high-performance thermoplastic PEEK is known for its excellent thermal and chemical resistance (Jones et al., 1985), making it highly

* Corresponding author.
E-mail address: florian.weber@iul.tu-dortmund.de (F. Weber).

https://doi.org/10.1016/j.aime.2025.100180
Received 16 September 2025; Received in revised form 1 December 2025; Accepted 30 December 2025
Available online 30 December 2025

suitable for joining applications. However, its mechanical behavior is strongly dependent on applied strain, strain-rate, and temperature. Below its glass transition temperature $T_g \approx 151$ °C (Drozdov and deClaville Christiansen, 2021), PEEK behaves as a viscoelastic-viscoplastic material, characterized by a nearly constant Young's modulus and pronounced strain hardening. Above T_g, both the yield stress and Young's modulus decrease significantly (Zheng et al., 2017). In addition, the mechanical response is strain-rate sensitive. Albérola et al. (1996) observed a significant increase in the apparent Young's modulus at strain-rates exceeding 1 s^{-1} by performing dynamic tensile testing over a strain-rate range of $5{\cdot}10^{-5}$ to 300 s^{-1} at room temperature. Similarly, Rae et al. (2007) showed that the initial yield stress increases nearly linearly with each logarithmic increment in strain-rate. Krishnaswamy and Kalika (1993) further demonstrated, using dynamic-mechanical-thermal analysis (DMTA), that PEEK relaxes only gradually across the glass–rubber transition, with a broad and slowly decaying relaxation attributed to the restricted mobility of the amorphous phase in the presence of crystallites. These factors support the selection of PEEK as the thermoplastic joining partner.

Joining these two materials presents a challenge due to their fundamentally different mechanical behavior. The joining of thermoplastics and metals via internal high-pressure expansion was first demonstrated by Han et al. (2022). In their work, composite pipes made of stainless steel and poly(vinyl chloride) were formed into threads through hydraulic expansion, which were then used to join two pipe ends. Based on membrane theory, the authors derived equations for calculating the required and maximum permissible fluid pressures. The influence of the joining partners' material behavior on the joint formation was not discussed. Further investigations by Weber et al. (2022) involved the joining of aluminum 6060 and polycarbonate tubes at their ends through hydraulic expansion. The authors reported that crazing in the amorphous polycarbonate during expansion did not affect the joint strength as measured in pull-out tests. However, they did not address whether this joint strength changes over time.

This paper aims to address this gap by employing a model experiment on joining-by-expansion to investigate the influence of thermoplastic material parameters on the joint strength. The materials are first characterized with respect to their mechanical behavior. Subsequently, the model experiment is used to investigate the influence of the maximum radial expansion during joining, the post-joining time, and the temperature of the joining partners during the process, on the resulting joint strength.

2. Materials

In the following, the materials of the joining partners are characterized with respect to their mechanical behavior. For this purpose, seamless extruded and drawn AA6061-T6 tubes with an outer diameter of $D_o = 50.8$ mm and a wall thickness of $s = 0.71$ mm are employed. From these semi-finished products, both the tensile specimens for material characterization and the ring samples for the model experiments are manufactured using laser beam cutting. The thermoplastic material used is PEEK, specifically the type Sustapeek-natural supplied by Röchling Group. The material was protected from direct sunlight and machined as received without thermal pretreatment to the dimensions of the respective test specimens. Starting from a base tube with dimensions $D_o = 70$ mm and $D_i = 50$ mm, both the specimens for mechanical characterization and the ring samples for the model experiments are machined to the final dimensions. The aluminum tensile specimens conformed to specimen geometry A80 as specified in DIN EN ISO 6892-1 (2019), while the PEEK specimens followed type 1BA according to DIN EN ISO 527-2 (2012). The ambient temperature T and relative humidity RH were recorded for all tests. An overview of the experimentally determined material properties of both joining partners is provided in Table 1.

Table 1
Mechanical properties of AA6061-T6 and PEEK.

AA6061 T6	Young's modulus E in GPa	Yield stress σ_0 in MPa	Ultimate tensile strength UTS in MPa		Elongation at break A in %
	69.8	271	320		11
PEEK	Young's modulus E in GPa	Yield strain ε_y in %	Elongation at break A in %		
			0.01 1/s	0.0037 1/s	0.00039 1/s
	4.01	4.4–4.9 %	16.0	17.9	24.4

2.1. Tensile test

The elastic-plastic behavior of the investigated materials is probed by means of uniaxial tensile tests conducted on a Z250 universal testing machine by Zwick/Roell (250 kN force capacity), whereby at least 5 repeat attempts were carried out for each parameter combination. For the curved aluminum specimens, specially designed curved grips were employed to ensure proper load application, which were integrated into the testing system. Since AA6061-T6 exhibits negligible strain-rate sensitivity in the quasi-static regime, the crosshead velocity was set to $2.5{\cdot}10^{-4}$ s^{-1} in accordance with the Standard, to accurately determine the Young's modulus E. After exceeding the initial yield stress the true strain-rate was increased to $6.7{\cdot}10^{-3}$ s^{-1} and maintained until specimen failure. Due to the limited gauge length of the 1BA specimen geometry, simultaneous use of longitudinal and transverse extensometers was not feasible, and strain-rate control could not be implemented. Instead, the crosshead velocity v_{TT} was varied between 0.025 and 2.5 mm/s.

During tension testing, AA6061-T6 exhibits a steep initial slope, followed by a pronounced yield point and moderate strain hardening (Fig. 1). In contrast, PEEK shows a lower initial stiffness and no distinct yield point, but rather a smooth transition into the plastic regime with a pronounced stress peak, followed by strain softening. The polymer exhibits strain-rate sensitivity, with higher testing velocities leading to increased engineering stresses.

The strain-rate associated with a constant crosshead velocity is illustrated in Fig. 2. To evaluate the strain-rate dependence of the Young's modulus E, the strain rate corresponding to each crosshead velocity was averaged over the interval $\varepsilon = 0.05$–0.25 %, i.e., the strain range used for modulus determination. For PEEK, no significant sensitivity of the Young's modulus E to the strain-rate was observed (Fig. 3), with an average value of 4.01 GPa with a standard deviation of 51 MPa. To determine the strain-rate dependence of the yield stress σ_y, the strain-rates shown in Fig. 2 were averaged up to ε_y, the corresponding yield strain. In contrast to E, both the yield stress σ_y and the yield strain ε_y

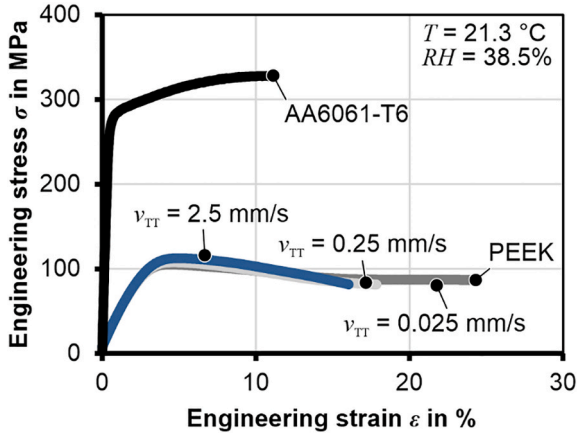

Fig. 1. Stress-strain behavior of AA6061-T6 and PEEK determined by tensile tests at room temperature.

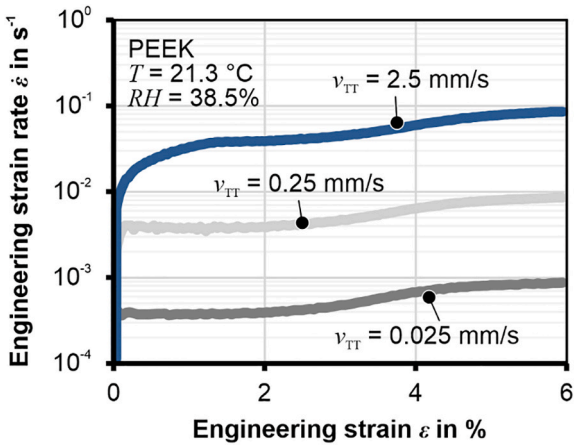

Fig. 2. Actual strain-rate of PEEK at room temperature in the tensile test at different crosshead velocities, which induce different average strain-rates.

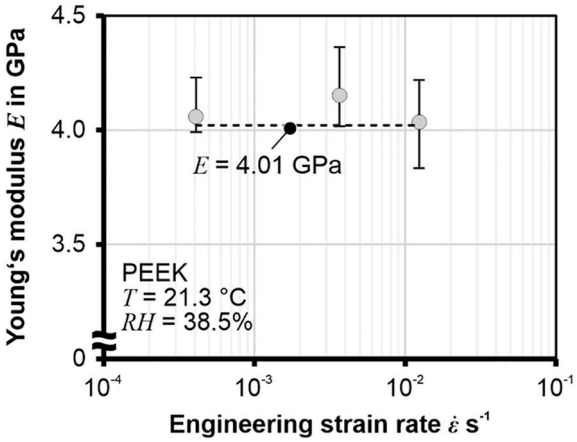

Fig. 3. Influence of strain-rate on the Young's modulus of PEEK at room temperature.

exhibited a logarithmic dependence on the strain-rate (Fig. 4). This behavior is consistent with the Eyring equation (Eyring, 1936), which describes yield kinetics by assuming that a chain segment moves to an adjacent vacant site by overcoming intra- and intermolecular resistances (Govaert et al., 2019). Accordingly, an increase in strain-rate requires a higher stress to achieve the same number of molecular transitions per unit time.

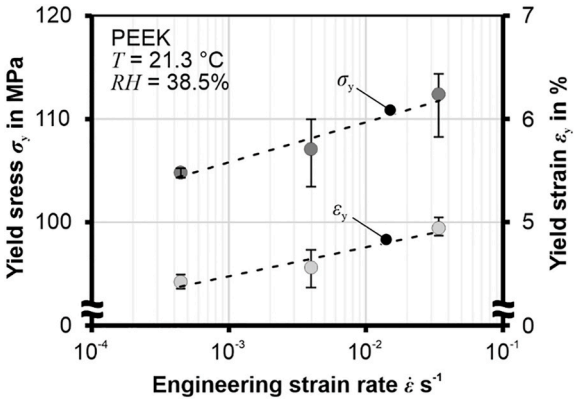

Fig. 4. Influence of strain-rate on the yield stress and strain of PEEK at room temperature.

2.2. Dynamic-mechanical-thermal analysis

In addition to the mechanical properties under quasi-static loading, a comprehensive understanding of the viscoelastic behavior of PEEK requires consideration of its temperature- and frequency-dependent material response. DMTA is conducted to characterize the time- and temperature-dependent behavior of the material within the linear viscoelastic regime. The DMTA experiments (Fig. 5) are performed on a Netzsch Gabo Eplexor 500 in accordance with DIN EN ISO 6721-1 (2019). The rectangular specimens, with a length of $l = 50$ mm and a cross-sectional area of $A_0 = 10$ mm^2, see Fig. 5, are machined from the previously described tubular semifinished product. To prevent buckling of the specimens during the dynamic loading phase, an initial static tensile strain of $\varepsilon_s = 0.1$ % is applied. An amplitude sweep at a chamber temperature of $T = 25.7$ °C and an angular frequency of $\omega = 6.28$ rad/s confirmed that the applied dynamic tensile strains in the range of $\varepsilon_d = \pm 0.002$ %–0.02 % remain within the linear viscoelastic range and do not induce nonlinear material behavior.

The temperature dependence of the material behavior is investigated in the range from $T = 25$–300 °C. The temperature sweep is carried out continuously with a heating rate of 2 K/min. Examination of the storage modulus E', which reflects the elastic energy stored and released during each cycle, reveals a plateau with only a slight decrease in modulus from room temperature up to approximately 150 °C (Fig. 6). Beyond this temperature, a pronounced drop in the storage modulus is observed, accompanied by a rise in both the loss modulus E'', representing the energy dissipated in each cycle as heat, and the loss factor $\tan\delta = E''/E'$, defined as their ratio and indicative of the material's damping behavior. Within the linear viscoelastic range, this behavior can be attributed to the thermal activation of large-scale chain motions in the amorphous regions of the polymer (Jonas and Legras, 1992). Note that at temperatures below the glass transition temperature of PEEK the loss moduli and the loss factor attain very low values causing pronounced statistical scatter.

To characterize the frequency dependence of the material behavior, frequency sweep tests are performed at constant temperatures with one specimen for each temperature. The angular frequency ω is varied in the range from 0.1 rad/s to 100 rad/s, starting with the highest frequency. The resulting storage modulus E', determined at different temperatures T, is plotted as a function of angular frequency ω in Fig. 7. At $T = 30$ °C, the storage modulus E' remains nearly constant under dynamic loading. Over the investigated frequency range, E' decreases by about 1.5 % from $\omega = 100$ rad/s to $\omega = 0.1$ rad/s. In contrast, at an elevated temperature

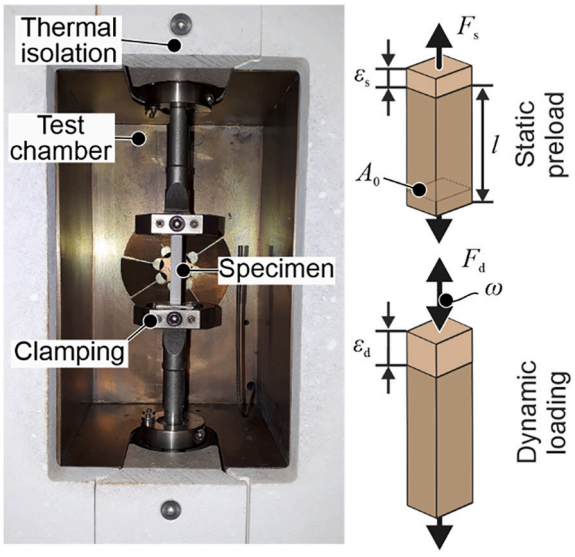

Fig. 5. DMTA test setup and the loading procedure.

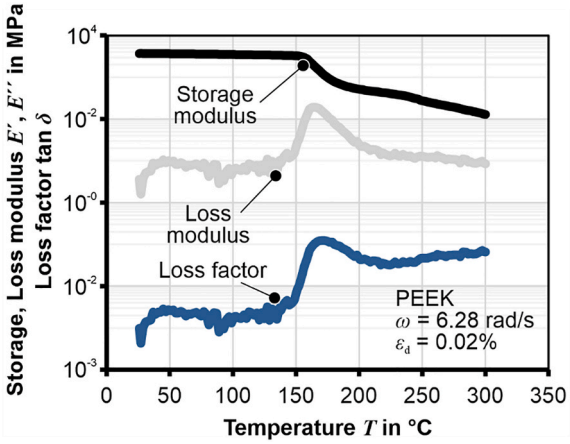

Fig. 6. Influence of temperature on storage modulus, loss modulus and loss factor of PEEK.

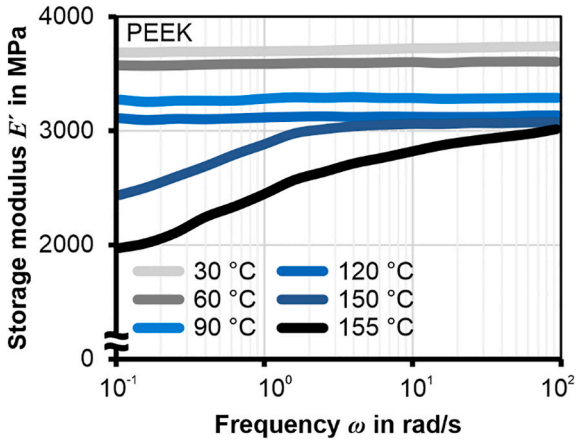

Fig. 7. Influence of angular frequency ω at different temperatures T on the storage modulus E'.

of $T = 155$ °C, the influence of the previously described thermally activated processes in PEEK becomes apparent. At this temperature, the storage modulus decreases by up to 35 % as a function of angular frequency.

2.3. Stress relaxation test

While DMTA investigations provide insights into the linear viscoelastic behavior over a range of frequencies and temperatures, stress relaxation experiments enable a targeted analysis of the time-dependent stress decay under constant strain. These experiments are conducted using a Shimadzu EZ-SX Texture Analyzer universal testing machine. The specimen geometry and preparation are identical to those used in the uniaxial tensile tests. The initial strain ε is applied using a crosshead displacement method at a velocity of $v = 10$ mm/min and is a variable in this investigation. In addition, the actual strain applied in the measurement range was determined using a 3D-DIC system Mini UX-100 by Photron. At t_0 the prescribed strain ε is attained, which gives rise to an initial stress σ that subsequently decays due to stress relaxation for $t > t_0$. The relaxation modulus is defined as the ratio of measured decaying stress σ at t_0 and the applied strain ε, while the relaxation time t_R is the total time t, subtracted by t_0. Fig. 8 presents the relaxations modulus E_R as a function of the relaxation time t_R for different initial strains ε. The total observation period for the relaxation tests is 10^4 s with three repetitions per parameter combination.

The data reveal a continuous decrease in E_R with increasing t_R ,

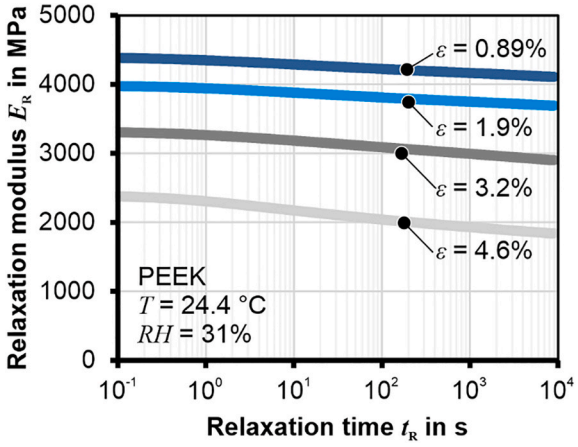

Fig. 8. Relaxation modulus of PEEK at room temperature.

indicating time-dependent stress relaxation even at room temperature, where the material remains in the glassy state. The magnitude of relaxation response increases systematically with strain. At low strain levels of $\varepsilon \leq 2.0$ %, the relaxation modulus decreases slightly over the observed time span, indicating a predominantly elastic response. At intermediate strains up to 3.2 %, a more pronounced reduction of E_R is observed. At higher strains $\varepsilon \geq 4.0$ %, the relaxation modulus drops markedly, reflecting enhanced stress relaxation due to increased molecular mobility and possible contributions from irreversible microstructural rearrangements.

For the quantitative assessment of stress relaxation, the measure $\Delta\sigma_R$ is introduced according to Eq. (2.1).

$$\Delta\sigma_R = \frac{\sigma(t_0) - \sigma(t)}{\sigma(t_0)} \tag{2.1}$$

Fig. 9 shows the progression of $\Delta\sigma_R$ for the entire period from 0 to 10^4 s in comparison to the observation period from 10^2 to 10^4 s. For the two considered time intervals, linear regression lines are determined. For the entire observation period, the relationship between relative stress relaxation $\Delta\sigma_R$ and strain ε is given by Eq. (2.2)

$$\Delta\sigma_R = 4.34 \cdot \varepsilon + 0.65 \tag{2.2}$$

For the interval from 10^2 s to 10^4 s, the regression according to Eq. (2.3) yields

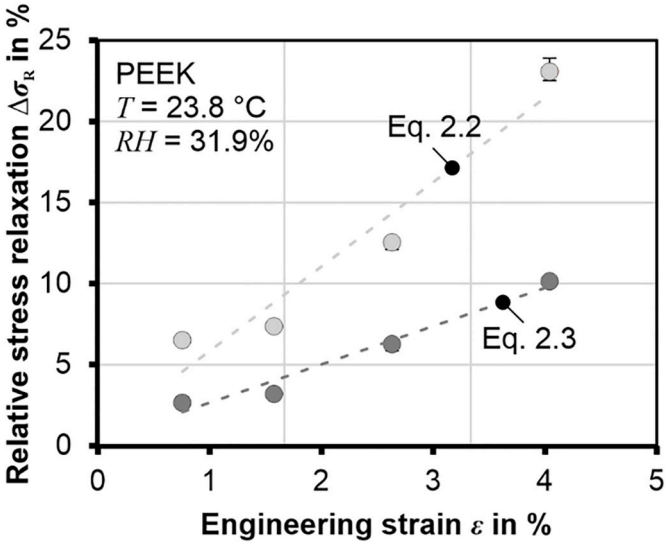

Fig. 9. Relative stress relaxation as a function of strain.

$$\Delta\sigma_R = 1.97 \cdot \varepsilon + 0.3 \quad (2.3)$$

The results show that the relative stress relaxation within the first 10^4 s increases with increasing strain. When only the relaxation between 10^2 s and 10^4 s is considered, the slope of the regression line is smaller. This behavior indicates that the stress relaxes more rapidly with increasing strain during the initial phase of relaxation.

3. Model experiment of joining by expansion

Joining-by-hydroforming is a process in which components are joined by expansion under internal pressure and is characterized by tensile stresses in the circumferential direction during loading in both joining partners as well as a permanent circumferential strain in the outer tube at the joining zone after joining, but depending on the required pressure level and application rate it can be technically demanding and challenging to implement on industrial equipment. To provide a more accessible representation of the underlying mechanisms, a simplified model experiment is introduced below. This experiment serves to illustrate the fundamental principle of internal high-pressure joining, which is accomplished through the co-expansion of the joining partners, and enables a controlled investigation of how the material properties of the polymer partner will affect the resulting force-fit. The concept underlying the model experiment has primarily been used to date for the characterization of materials in circumferential stress and strain states. Reference is made here to the work of Nilsson et al. (2011) on the characterization of zircaloy and Cui et al. (2025) on 304 stainless steel and AA6061.

3.1. Experimental setup

The model experiment consists of joining two, concentrically-placed ring specimens by the separated-expansion-mandrel test (SEMT) (Fig. 10a), and the subsequent testing of the resulting joint by the push-out test (POT) (Fig. 11). The joining process is carried out using a set of eight additively manufactured expansion segments made of 316L stainless steel with a yield stress of 500 MPa and a Young's modulus of 180 GPa (Rosenthal, 2022), and an octagonal pyramidal punch featuring an angle $\alpha = 14.84°$, identical to that of the inner faces of segments and made of 42CrMo4 steel (Fig. 10b). The segments outer surface matches the curvature of the inner surface of the aluminum tube and they are free to move in the radial direction, but not in the other two.

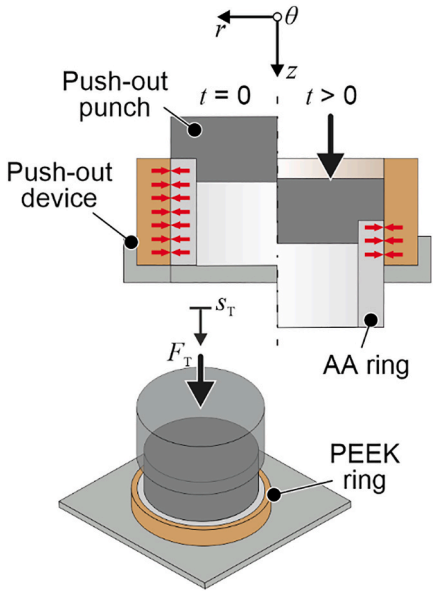

Fig. 11. Setup of the POT.

At the start of the SEMT, the expansion punch is driven vertically along the displacement path s_J, which lies on the common axis of the expansion segments and the concentric rings, to the maximum position at which no force F_J is detected (Fig. 10c). Upon contact of the punch with the corresponding flat inner surfaces of the expansion segments, a radial outward movement of the segments is induced. This horizontal displacement causes the segments to engage the concentrically-positioned rings, made of AA6061-T6 and PEEK, respectively. The rings then co-expand, thereby mimicking the homogenous expansion induced by hydraulic pressure in the actual application. After a predefined punch stroke is reached, corresponding to the desired radial expansion, the punch retracts to its initial position, allowing the joined rings to undergo elastic springback. For the test series examining the influence of temperature T on the joint strength, the assembled system of expansion elements and rings is preheated in a furnace. The radial force required for expansion of the rings cannot be controlled during expansion because the contact area between the aluminum ring and the

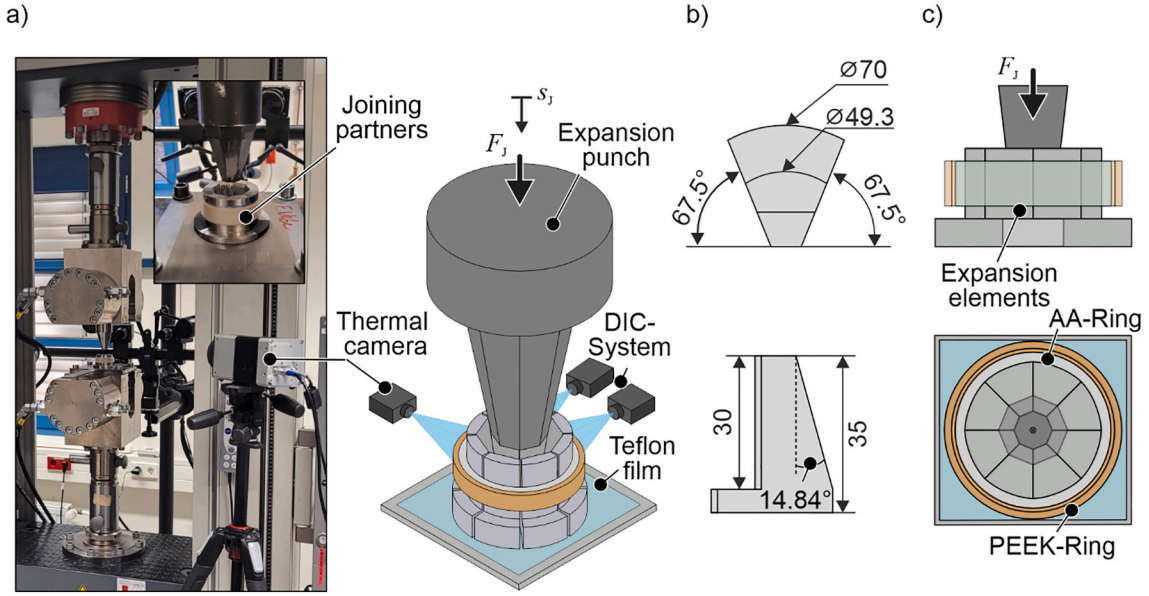

Fig. 10. a) Joining setup, b) dimensions of the expansion dies and c) initial positioning of the tools and specimen and of the SEMT.

expansion element changes continuously. Therefore, the process cannot be directly transferred to internal high pressure joining, where a homogeneous internal pressure expands an aluminum tube. For this reason, the circumferential strain on the outer surface of the PEEK ring is measured by optical means using the stereo digital image correlation system Aramis 5M from Zeiss. The resulting data can be transferred to internal high pressure joining as long as the expansion of the ring remains approximately homogeneous in the circumferential direction. The temperature of the outer ring during expansion is recorded using a thermal imaging camera VarioCam HD head 680 by Infratec. A total of five tests are performed per parameter combination.

In the second step, the joint strength of the assembled rings is evaluated by the POT (Fig. 11). The joined ring assembly is placed into a test fixture, with the PEEK ring positioned on a defined shoulder and fixed in both the horizontal and vertical directions to prevent any movement during testing. The push-out punch is designed with inner and outer diameters matching those of the aluminum ring to ensure uniform loading. The punch is then driven at a constant velocity of $v_T = 0.5$ mm/s, applying a punch force F_T directly on the aluminum ring.

The aluminum rings are manufactured by laser cutting from extruded tubes and feature an inner diameter of $D_i = 49.7$ mm, an outer diameter of $D_o = 50.8$ mm, and a height of $h = 15$ mm. The PEEK rings are turned from the same base material used in the previous material characterization and have an inner diameter of $D_i = 51$ mm, an outer diameter of $D_o = 55$ mm, and a height of $h = 15$ mm. That means that the radial clearance between AA and PEEK is 0.1 mm, or 0.2 % of the outer diameter of the AA ring. The inner surface of the PEEK rings and the outer surface of the AA6061 rings is measured tactilely with a MarSurf XR1 by Mahr at three positions around the circumference after manufacturing and before the start of the test. The aluminum rings have an average roughness of $R_z = 5.24$ µm, while the surface of the PEEK rings has a value of $R_z = 7.58$ µm.

3.2. Limitations of the model experiment

The segmentation of the eight expansion elements, combined with friction at the interface between the segments and the aluminum ring, lead to a non-axisymmetric deformation of the assembly. Measurements obtained with a VR-5200 3D profilometer from Keyence, shown in Fig. 12, reveal that the resulting roundness deviation is hardly detectable at small punch strokes of $s_J = 2$ and 4 mm, but becomes clearly visible at $s_J = 8$ mm.

The DIC measurements are performed along an arc in the cylindrical coordinate system in the circumferential direction and perpendicular to it in the axial direction of the rings (Fig. 13). To assess the complex strain state at the maximum punch displacement of 8 mm the expansions of the aluminum ring and the PEEK ring must be considered separately. In the aluminum ring the internal pressure p_i acts on the segment due to contact with the expansion element, generating a radial stress σ_r. Circumferential tensile stresses σ_θ arise as the ring expands and an axial tensile stress state σ_z also develops which is generated by friction between the tool and the ring. This friction opposes axial compression ε_z and produces a compressive thickness strain ε_t as (Cui et al., 2025). In the opening gap the ring is straightened by a prevailing bending moment (Jiang and Wang, 2018). Because there is no friction between the expansion element and the ring in this region the thickness reduction ε_t is smaller and the axial compression ε_z is larger than on the segment. In the PEEK ring the segment is subjected to a contact pressure p_c due to contact with the aluminum ring, causing a radial stress σ_r that decays with the radius of the ring, as well as axial tensile stresses σ_z arising from friction between the two joining partners. Due to the straightening of the aluminum ring across the gap, either no contact forms between the PEEK and aluminum rings in this region, or any contact there carries a lower pressure than on the adjacent segment. This increases axial compression ε_z in the gap compared with the segment. With respect to the circumferential strain ε_θ maximum values appear at the edge of the opening gap which result from the superposed bending moment caused by straightening in the gap. This trend is also evident in the DIC measurements in Fig. 13. Due to the nonuniform reduction in thickness an inhomogeneous distribution of the contact pressure p_c develops along the ring circumference. Consequently, transferring these results to internal high pressure joining where a homogeneous expansion leads to a homogeneous contact pressure over the circumference is no longer possible as the strain distribution becomes increasingly inhomogeneous. This inhomogeneity also influences the springback of the joining partners. In theory, springback in internal high-pressure joining in the joining zone consists of the elastic springback of the inner joining partner and its elastic compression due to the contact pressure acting after joining. Since the contact pressure is distributed inhomogeneously, the springback of the aluminum ring in the model experiment does not correspond to that of a homogeneously expanded ring.

This strain inhomogeneity becomes more pronounced with increasing radial expansion. The deviation of the circumferential strain from the mean value increases with increasing punch stroke s_J, see Fig. 14.

Based on the initial geometric configuration (Fig. 15), an apparent circumferential strain $\varepsilon_{\theta,A}$ is calculated as a function of the vertical displacement of the expansion punch s_J. Equation (4.1) first determines the punch displacement required to overcome the initial joining gap a_0

$$s_{J,a_0} = \frac{a_0}{\tan \alpha} \tag{4.1}$$

as a function of the angle α. For the geometry used in this work, $s_{J,a_0} = 0.38$ mm. The apparent circumferential strain is then obtained by Eq. (4.2) by dividing the radial expansion Δr by the initial outer radius r_0, considering that a portion of the punch stroke was already used to close the joining gap.

$$\varepsilon_{\theta,A} = \frac{\Delta r}{r_0} = \frac{(s_J - s_{J,a_0}) \tan \alpha}{r_0} \tag{4.2}$$

Comparing the apparent circumferential strain $\varepsilon_{\theta,A}$ with the engineering circumferential strains ε_θ reveals the onset of strain

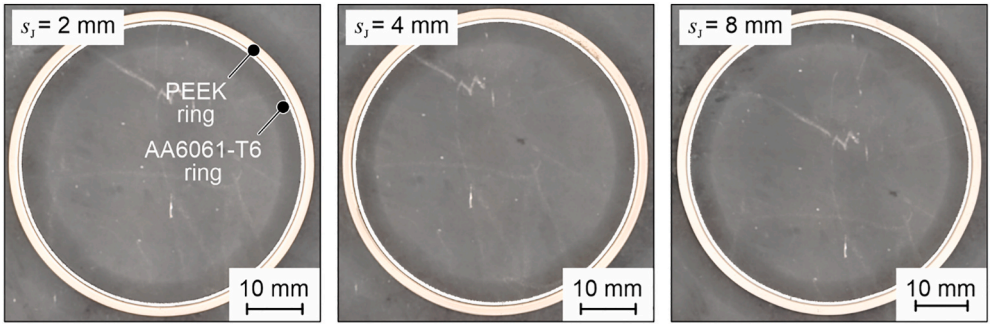

Fig. 12. Profilometer images of joined rings with different punch strokes s_J.

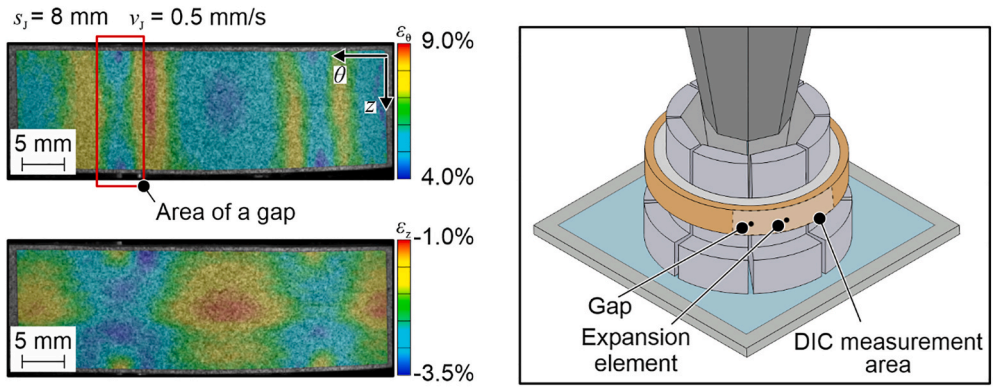

Fig. 13. Optically determined circumferential and axial strains at the outer surface of the PEEK. ring, at the maximum punch stroke during joining and resulting stress and strain state in the joining partners.

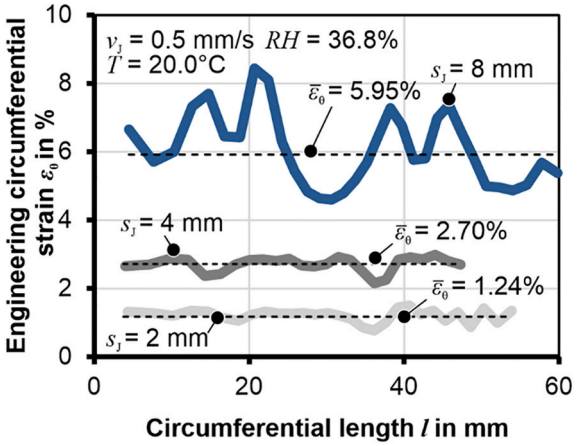

Fig. 14. Circumferential strain ε_θ for different punch strokes s_J.

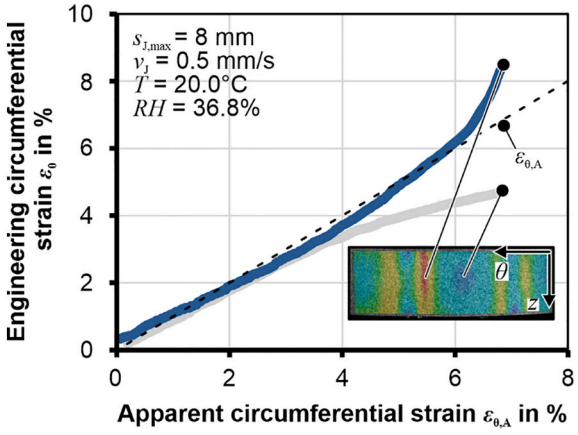

Fig. 16. Engineering circumferential strain as a function of apparent circumferential strain.

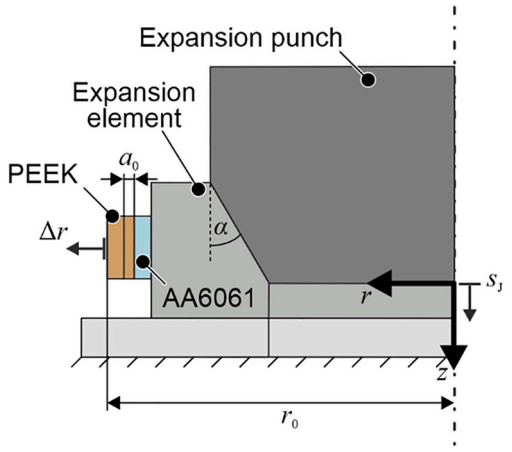

Fig. 15. Geometric relationship between expansion tools and ring expansion.

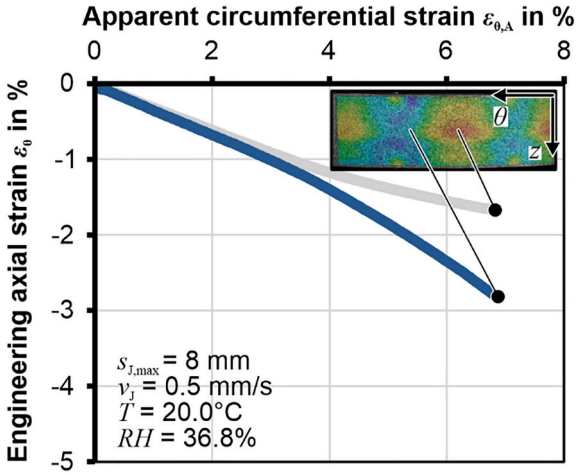

Fig. 17. Engineering axial strain as a function of apparent circumferential strain.

inhomogeneity at approximately 3.7 % (Fig. 16). This corresponds to a punch displacement of $s_J = 4.22$ mm.

Beyond this punch stroke, an emerging inhomogeneity of the strain distribution can also be observed in the axial direction (Fig. 17). A higher negative axial strain is observed at the segment edge compared to the region on the segment.

The onset of the strain inhomogeneity is also reflected in the evolution of the circumferential strain-rate (Fig. 18), which remains at an average value of 0.0043 s^{-1} up to an apparent circumferential strain of 3.7 %. Accordingly, it can be concluded that a largely homogeneous circumferential strain state is achieved below an apparent circumferential strain of 3.7 %, or a punch displacement of 4.22 mm. After that, the straining becomes spatially inhomogeneous, with some regions stretching further whereas others are unloading elastically.

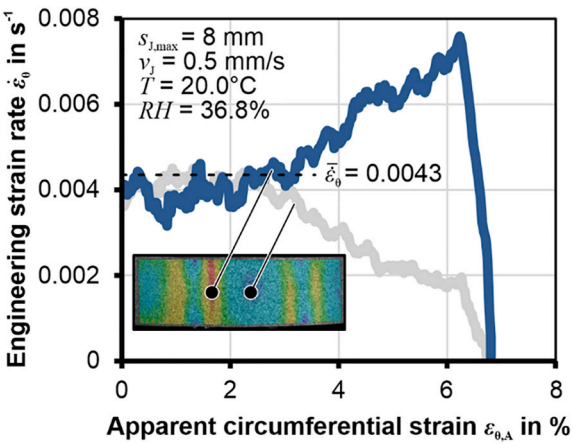

Fig. 18. Engineering circumferential strain rate as function of apparent circumferential strain.

4. Results and discussion

4.1. Influence of applied circumenferential strain on the joint strength

Joining by expansion is carried out using punch strokes s_J of 2, 4, and 8 mm, which results in the average circumferential strains $\bar{\varepsilon}_\theta$ shown in Fig. 14. The resulting joints are subsequently tested at room temperature using a punch velocity $v_T = 0.5$ mm/s. The time interval between the joining process and mechanical testing is $t_D = 100$ s.

The force displacement curves from the POT (Fig. 19) initially show a steep increase in punch force F_T at small punch strokes s_T. This initial rise is governed by static friction at the interface of the joining partners, and the slope of the rise reflects the combined stiffness of the testing machine and the joined ring assembly. After reaching a maximum, F_T decreases with increasing punch stroke. The force maximum indicates the onset of macroscopic relative motion between the rings, which corresponds to a transition from static to sliding friction. The subsequent decrease is primarily due to the progressively diminishing load bearing contact area as the aluminum ring is pushed out of the surrounding PEEK ring. During this phase, tilting of the inner aluminum ring may occur, which can be triggered by locally nonuniform contact pressure acting on the aluminum ring during push-out, requiring the punch to be displaced beyond the height of the PEEK ring in order to fully separate the components. This leads to relative punch displacements $s_T/h > 1$, shown exemplarily in Fig. 19 for strokes of 4 and 8 mm.

Exceeding the maximum push-out force $F_{T,max}$ is defined as the failure of the force-fit of the joint. The parameter for joint strength σ_J is defined according to Eq. (4.3) as the ratio of this maximum force to the apparent cross-sectional A_0 area of the aluminum ring after joining, which in turn is derived from the geometrical relations given in Fig. 15.

$$\sigma_J = \frac{F_{T,max}}{A_0} \tag{4.3}$$

The joint strength σ_J, normalized by the yield stress σ_y of the softer material PEEK, increases with rising average circumferential strain $\bar{\varepsilon}_\theta$ (Fig. 20). Between an average strain of 1.24 % and 5.95 %, the slope of this increase changes, and the rate of growth becomes less pronounced. The authors attribute this change to the onset of plasticization in the PEEK ring. From an apparent circumferential strain $\varepsilon_{\theta,A} = 3.7$ % onward, the inhomogeneity of the circumferential strain distribution increases, reaching an average of 5.95 % at a punch displacement of $s_J = 8$ mm. This value is above the yield strain $\varepsilon_y = 4.73$ % determined from the uniaxial tensile test. This demonstrates that the upper limit proposed by Marré (2009) in the context of joining-by-hydroforming, beyond which the outer joining partner undergoes plastic deformation, is also relevant for joining by expansion of AA6061-T6 and PEEK.

4.2. Influence of the stress relaxation on the joint strength

To assess the extent to which the joint strength σ_J after forming is influenced by time-dependent effects due to the viscoelastic behavior of PEEK, the time interval t_D between joining and testing is varied between 10^2 s and 10^5 s. Time intervals $t_D < 10^2$ s could not be realized, as safe removal from the joining setup, transfer to the testing setup, and positioning of the push-out punch in its initial position cannot be reliably ensured within shorter durations.

The normalized joint strength σ_J decreases with increasing expansion time t_D (Fig. 21). For the tested circumferential strains of 2.70 % and 5.95 %, a plateau is reached after approximately 10^4 s, indicating the establishment of an equilibrium state. This behavior cannot be confirmed for the strain level of 1.24 %. The reason for this is attributed to the experimental accuracy, as represented by the error bars. The absolute error across all joint strength measurements is ± 90 N. According to Eq. (2.3), at a mean circumferential strain of 1.24 %, the expected relative relaxation is approximately 2.57 % between 10^2 s and 10^4 s and corresponds to a decrease of about 28 N. This reduction lies within the experimental scatter. Therefore, an equilibrium state cannot be demonstrated. Since the experimental error does not scale proportionally with the applied strain, the relative uncertainty becomes more pronounced at small strains. When analyzing the joint strength at strains of 2.70 % and 5.95 %, it is further observed that the strength increase due to enhanced expansion is entirely diminished with increasing t_D, resulting in a comparable joint strength for both expansion levels. This

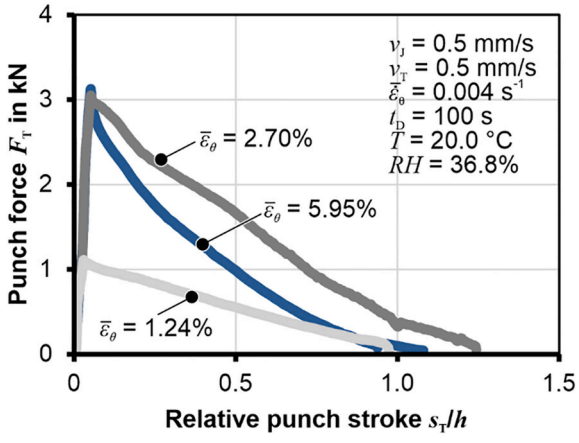

Fig. 19. Push-out force during testing of the joint for different expansions.

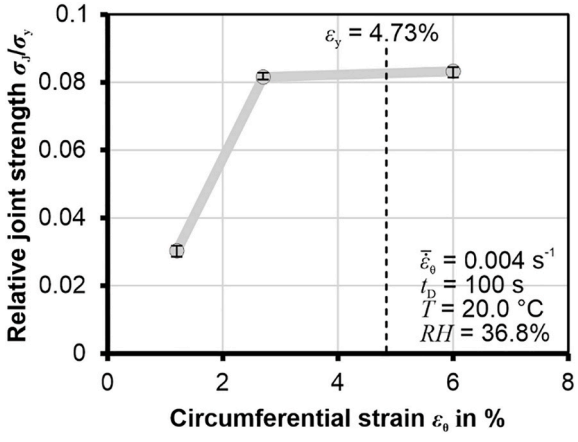

Fig. 20. Joint strength as a function of applied circumferential strain on the PEEK.

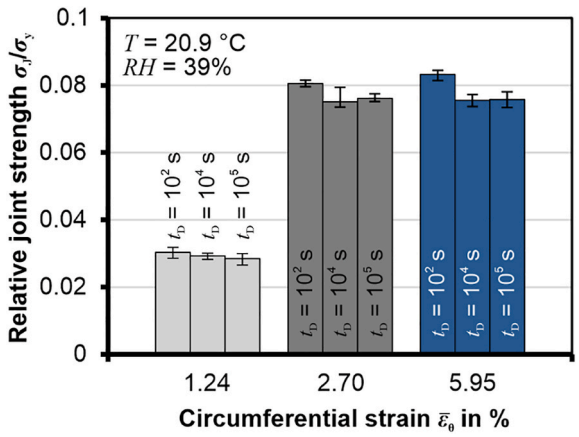

Fig. 21. Decay in joint strength over time for different expansions.

observation is attributed to irreversible microstructural rearrangements and the resulting more pronounced stress relaxation at higher strains in Fig. 8.

The decrease in joint strength with increasing time t_D can be attributed to the stress relaxation of PEEK. After joining, the PEEK ring cannot elastically spring-back to its original shape due to the plastic expansion of the aluminum ring, resulting in a constant circumferential strain being applied to the PEEK ring. This constant strain leads to a reduction in stress within the PEEK over time. A comparison of the decrease in joint strength between 10^2 s and 10^4 s (Fig. 21) with the results of the stress relaxation tests (Fig. 9) and the linear regression according to Eq. (2.3) reveals a clear correlation between these quantities (Fig. 22) for strains below the yield strain. At a strain of 5.95 % the deviation is more pronounced, which indicates that a linear relationship between stress relaxation and strain is only appropriate for strains within the elastic range of the material.

4.3. *Influence of the joining temperature on the joint strength*

When conducting joining at elevated temperatures, potentially beneficial effects may arise from thermal compression upon cooling, since the thermal expansion coefficient of PEEK below its glass transition temperature is approximately $60{\cdot}10^{-6}$ K^{-1} (Lu et al., 1996), whereas AA6061-T6 exhibits a considerably lower coefficient of about $21{\cdot}10^{-6}$ K^{-1} (Sharma) in the same temperature range. In addition, enhanced softening of PEEK at elevated temperature (Lin et al., 2019) promotes interfacial changes and micromechanical interlocking due to deeper penetration of AA6061 surface asperities into the polymer, which can

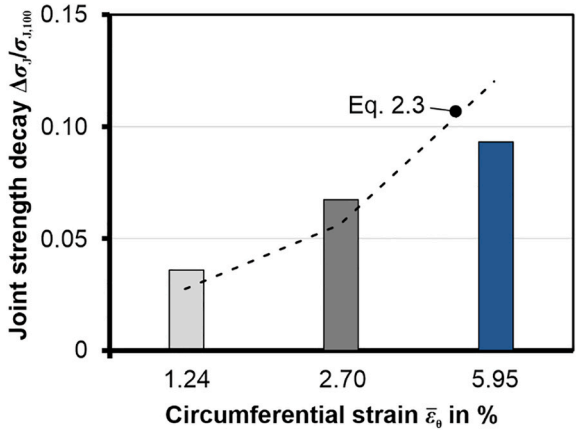

Fig. 22. Decay in joint strength σ_J between 10^2 and 10^4 s compared to the relaxation test data shown in Fig. 9.

restrain relative displacement and thereby increase joint strength. Conversely, adverse effects are associated with the reduction of the storage modulus of PEEK and the decrease of the Young's modulus of aluminum with increasing temperature (Roy et al., 2022). The subsequent analysis aims to clarify which of these effects are dominant.

To investigate the influence of workpiece temperature on joint strength, the rings, including the expansion elements, are heated in their assembled state in a furnace. The setup is heated to the target temperature T_0 and held in the furnace for 20 min (Fig. 23). Three furnace temperatures of T_0 = 100, 120, and 140 °C are considered in the investigations. It is then removed and positioned immediately in the test space of the universal testing machine. During this transfer, the setup cools to temperature T_1, which is measured on the outer surface of the PEEK ring using a thermal imaging camera. The temperature distribution along the circumference and height of the PEEK ring is uniform (Fig. 23). Subsequently, the expansion punch is moved to its initial position with a velocity of 10 mm/s, at which point the PEEK ring has cooled to a temperature of T_2. The punch is then advanced by a displacement of s_J = 4 mm. Upon reaching the maximum punch displacement, the temperature T_3 is recorded. Finally, the joined rings cool naturally by convection to room temperature of approximately 22.1 °C.

Considering the temperatures measured on the outer surface of the PEEK ring at the previously defined time points in Fig. 23, the temperature decreases due to the cooler ambient temperature in the test setup are 18.8 % (from 140 °C to T_3), 19.1 % (from 120 °C to T_3), and 16.1 % (from 100 °C to T_3) (Fig. 24).

Using the light microscopy images (Fig. 25), the transition zone between the two joining partners is analyzed. AA6061-T6, due to its face-centered cubic (FCC) crystal structure, exhibits colorful grain contrast in the micrographs, whereas PEEK remains insensitive to the polarized light filter. The observations reveal a smooth interface between AA6061-T6 and PEEK at room temperature. With increasing joining temperature, the interface becomes rougher, and at T_0 = 140 °C, localized micro-undercuts are observed.

To exclude the possibility that heating to T_0 for 20 min affected the peak-aged condition of AA6061-T6, hardness measurements are conducted at room temperature in the as-received condition and after a heat treatment of 140 °C for 20 min. The hardness measurements (HV5) yield values of 94.8 (as-received) and 94.9 (T_0 = 140 °C). As shown in Fig. 23, the thermal cycle in the joining experiment also includes transport from the furnace to the joining setup and the joining process itself. Since these

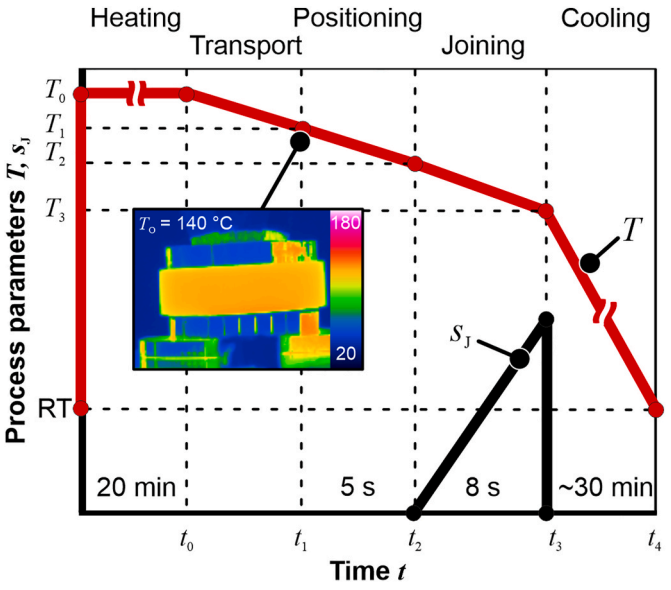

Fig. 23. Temperature profile for joining at elevated temperatures.

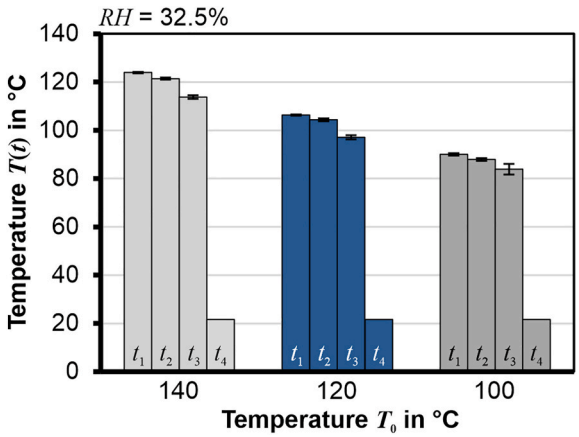

Fig. 24. Measured temperatures throughout the test.

time intervals only last a few seconds, it can be assumed that the thermal history of the AA rings in the hardness measurements is the same as that in the model experiment. It can therefore be concluded that heating did not alter the T6 condition significantly, and consequently no influence of the AA6061-T6 state on the joining result is expected.

After joining in the heated condition, the rings are cooled for a duration of $t_D = 10^4$ s. The subsequent push-out tests reveal a decreasing trend of the maximum force with increasing joining temperature (Fig. 26). It can be concluded that the negative effects of elevated temperature outweigh the positive ones with respect to the contribution of temperature to the force-fit.

An increase in the temperature of the joining partners leads to a reduction in the Young's modulus of aluminum. Summers et al. (2015) reported a decrease of approximately 5 %, while Roy et al. (2022) observed a reduction of about 15 % at 150 °C. Such a decrease in the Young's modulus of the inner joining partner is unfavorable for force-fits, as it increases the elastic springback of the inner ring and thereby reduces the constraint imposed on the springback of the outer partner. As a result, the contact pressure between both partners is lowered, which in turn reduces the joint strength, despite the larger cooling shrinkage of PEEK over AA6061-T6.

DMTA results show a decrease in the storage modulus of PEEK with increasing temperature, see Fig. 6. The relative loss in push-out force mirrors the relative reduction in storage modulus, see Fig. 27. This agreement indicates that the temperature driven decrease of the PEEK storage modulus is the dominant driver of the deterioration of the force fit at elevated temperatures. In contrast, the model experiment does not permit a reliable quantification of the contributions from the increased springback of AA6061 due to its lower Young's modulus at higher temperature and from thermal compression during cooling because the contact pressure is nonuniform and full contact between the rings is not guaranteed.

5. Conclusion and outlook

A model experiment was developed to enable a straightforward investigation of expansion-based joining in a well-controllable experimental environment. This approach was used to study the influence of PEEK expansion, represented by the engineering circumferential strain, along with stress relaxation in PEEK and the temperature of the joining partners, on the resulting joint strength. PEEK exhibits, with increasing strain, initially linear elastic, then non-linear elastic, and finally plastic deformation behavior. This transition affects the joining process such that the gain in joint strength diminishes once the elastic limit is exceeded. While this transition effect was already known for metallic joints and is utilized in industrial applications, this effect was confirmed in these investigations for metal-polymer joints.

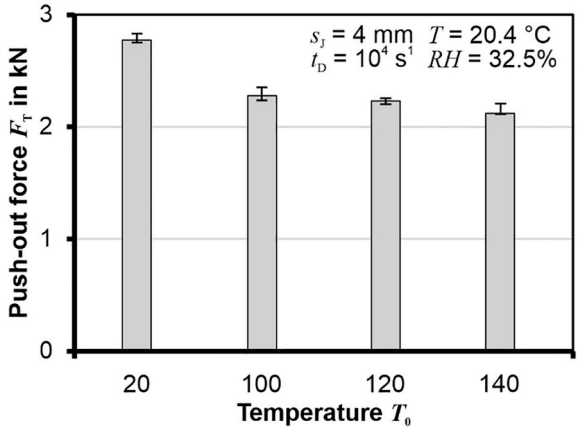

Fig. 26. Push-out force as a function of furnace temperature.

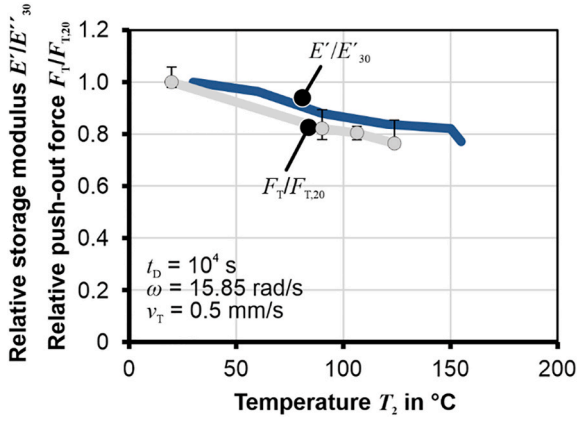

Fig. 27. Decay in joint strength as a function of joining temperature compared to DMTA data from Fig. 6.

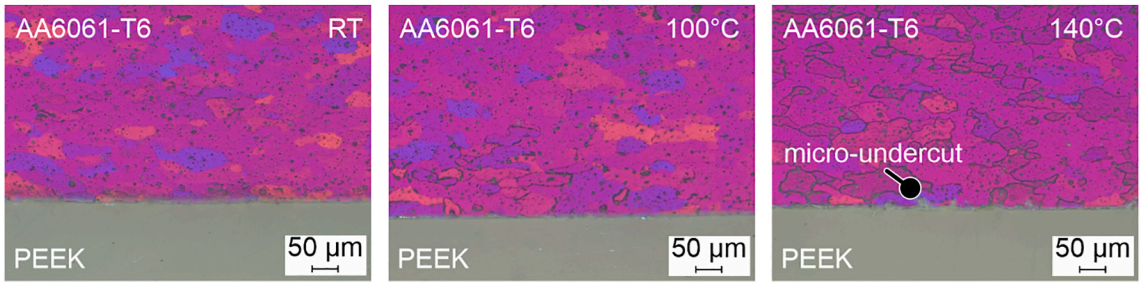

Fig. 25. Scanning electron micrographs of the joining area at room temperature and after heating to different furnace temperatures.

Stress relaxation in PEEK also increases with strain and, as a result, the joint strength decreases over time. Expansion beyond the elastic limit of PEEK does not improve the final equilibrium joint strength after 10^4 s. When using metal-polymer joints that are joined by interference-fit, in which the polymer joining partner is subjected to constant strain after joining, the decrease in joint strength over time should therefore be taken into account in the industrial design of the joint.

Increasing the temperature of the joining partners adversely affects the connection. Heating to 140 °C results in a 13.6 % reduction in joint strength compared to room temperature, following the trend of the PEEK storage modulus decrease. This suggests that a lower elastic energy in the polymer reduces the force-fit. Furthermore, the Young's modulus of aluminum decreases with temperature, which further weakens the joint. Therefore, if the process is intended to exploit the higher plastic formability of PEEK while maintaining a force-fit, only the PEEK should be heated. Based on the time–temperature superposition principle, it can also be concluded that reducing the temperature and thereby increasing the strain rate would improve joint strength.

The findings will be used to define the process parameter space for joining-by-hydroforming, thereby facilitating experimental implementation. In addition, the insights into relevant material and process parameters will serve as the basis for developing an analytical model to predict the joint strength. In the context of industrial implementation such as joining by hydroforming, however, increasing the strain rate by applying the fluid more quickly appears to be easier to implement and more effective than the temperature route.

CRediT authorship contribution statement

Florian Weber: Writing – original draft, Methodology, Investigation, Conceptualization. **Ulrich A. Handge:** Supervision, Investigation. **Tanmoy Rakshit:** Investigation. **Hamed Dardaei Joghan:** Writing – review & editing. **Marlon Hahn:** Writing – review & editing. **Yannis P. Korkolis:** Writing – review & editing, Supervision. **A. Erman Tekkaya:** Writing – review & editing, Supervision, Methodology, Funding acquisition, Conceptualization.

Declaration of generative AI and AI-assisted technologies in the manuscript preparation process

During the preparation of this work the authors used ChatGPT5 in order to check and improve the readability of the article. After using this tool, the authors reviewed and edited the content as needed and take full responsibility for the content of the published article.

Declaration of competing interest

The authors declare that they have no known competing financial interests or personal relationships that could have appeared to influence the work reported in this paper.

Acknowledgements

This research was funded by the German Federal Ministry of Economic Affairs and Energy (Project: AutoFit, project number: 20W1905D). The authors would like to thank Martin Krol and Christoph Klippenstein for their support in conducting the joining experiments, Gunnar Windisch for his assistance in designing the model experiment, and Pascal Brech and Lars Schega for their contribution to the characterization of the PEEK material.

Data availability

Data will be made available on request.

References

Agarwal, H., Gokhale, A.M., Graham, S., Horstmeyer, M.F., 2003. Void growth in 6061-aluminum alloy under triaxial stress state. Mater. Sci. Eng., A 341, 35–42.
Albérola, N.D., Mélé, P., Bas, C., 1996. Tensile mechanical properties of PEEK films over a wide range of strain rates. II. J. Appl. Polym. Sci. 64, 1053–1059.
Amancio-Filho, S.T., dos Santos, J.F., 2009. Joining oy polymers and polymer-metal hybrid structures: recent developments and trends. Poylmer Engineering and Science 49 (8), 1461–1476.
Balle, F., Wagner, G., Eifler, D., 2009. Ultrasonic metal welding of aluminium sheets to carbon fibre reinforced thermoplastic composites. Adv. Eng. Mater. 11. https://doi.org/10.1002/adem.200800271.
Cui, X.-L., Sun, Q., Wang, Y., Yuan, S., 2025. Measurement and calculation method for circumferential plastic strain ratio of anisotropic aluminum alloy tubes. Int. J. Solid Struct. 313. https://doi.org/10.1016/j.ijsolstr.2025.113311.
DIN EN ISO 527-2, 2012. Plastics – Determination of Tensile Properties – Part 2: Test Conditions for Moulding and Extrusion Plastics. Beuth-Verlag GmbH, Berlin.
DIN EN ISO 6721-1, 2019. Plastics – Determination of Dynamic Mechanical Porperties – Part 1: General Principles.
DIN EN ISO 6892-1, 2019. Metallic Materials – Tensile Testing – Part 1: Methods of Test at Room Temperature. Beuth-Verlag GmbH, Berlin.
Drozdov, A.D., deClaville Christiansen, J., 2021. Thermo-Mechanical behavior of Poly (ether ether ketone): experiments and modeling. Polymers 13. https://doi.org/10.3390/polym13111779.
Eyring, H., 1936. Viscosity, plasticity, and diffusion as examples of absolut reaction rates. J. Chem. Phys. 4. https://doi.org/10.1063/1.1749836.
Govaert, L.E., Vegt, A.K., van der Vegt, M., Drongelen, van, 2019. Polymers: from Structures to Properties. Delft Academic Press, Niederlande.
Hahn, M., Gies, S., Tekkaya, A.E., 2019. Light enough or go lighter. Mater. Des. 163. https://doi.org/10.1016/j.matdes.2018.107545.
Han, S.W., Kim, D., Abolhasani, D., VanTyne, C.J., Moon, Y.H., 2022. Joining of metal-plastic composite layered tubes by hydroformed threaded coupling. J. Manuf. Sci. Eng. 144. https://doi.org/10.1115/1.4054870.
Jiang, H., Wang, J.-A.J., 2018. Development of cone-wedge-ring-expansion test to evaluate the tensile HOOP properties of nuclear fuel cladding. Prog. Nucl. Energy 108. https://doi.org/10.1016/j.pnucene.2018.06.015.
Jonas, A., Legras, R., 1992. Relation between PEEK semicrystalline morphology and its subglass relaxations and glass transition. Macromolecules 26 (S), 813–824.
Jones, D.P., Leach, D.C., Moore, D.R., 1985. Mechanical properties of poly(ether-ether-ketone) for engineering applications. Polymer 26, 1385–1393.
Krishnaswamy, R.K., Kalika, D.S., 1993. Dynamic mechanical relaxation properties of poly(ether ether ketone). Polymer 35 (6), 1157–1165.
Lin, L., Pei, X.-Q., Bennewitz, R., Schlarb, A.K., 2019. Tribological response of PEEK to temperature induced by frictional and external heating. Tribol. Lett. 67 (52). https://doi.org/10.1007/s11249-019-1169-4.
Lu, S.X., Cebe, P., Capel, M., 1996. Thermal stability and thermal expansion studies of PEEK and related polyimides. Polymer 37 (14), 2999–3009.
Marré, M., 2009. Grundlagen Der Prozessgestaltung Für Das Fügen Durch Weiten Mit Innenhochdruck. TU Dortmund University, Germany. PhD-Thesis.
Nilsson, K.-F., Martin, O., Chenel-Ramos, C., Mendes, J., 2011. The segmented expanding cone-mandrel test revisited as material characterization and component test for fuel claddings. Nucl. Eng. Des. 241. https://doi.org/10.1016/j.nucengdes.2010.10.026.
Rae, P.J., Brown, E.N., Orler, E.B., 2007. The mechanical properties of poly(ether-ether-ketone) (PEEK) with emphasis on the large compressive strain response. Polymer 48 (S), 598–615.
Rosenthal, R., 2022. Umformung Additive Gefertigter Bleche Mit Strukturiertem Kern. TU Dortmund University, Germany. PhD-Thesis.
Roy, B.K., Korkolis, Y.P., Arai, Y., Araki, W., Iijima, T., Kouyama, J., 2022. Plastic deformation of AA6061-T6 at elevated temperatures: experiments and modeling. Int. J. Mech. Sci. 216. https://doi.org/10.1016/j.ijmecsci.2021.106943.
Scapin, M., Manes, A., 2018. Behaviour of Al6061-T6 alloy at different temperatures and strain-rates: experimental characterization and material modelling. Mater. Sci. Eng., A 734, 318–328.
Sharma, S. C., Effect of albite particles on the coefficient on thermal expansion behavior of the AA6061 alloy composites. Metall. Mater. Trans. A, 31, DOI: https://doi.org/10.1007/s11661-000-0019-0.
Summers, P.T., Chen, Y., Rippe, C.M., Allen, B., Mouritz, A.P., Case, S.W., Lattimer, B.Y., 2015. Overview of aluminum alloy mechanical properties during and after fires. Fire Science Reviews 4. https://doi.org/10.1186/s40038-015-0007-5.
Weber, F., Lehmenkühler, P., Hahn, M., Tekkaya, A.E., 2022. Joining of metal-thermoplastic-tube-joints by hydraulic expansion. Proceedings of the ASME 2022 17th International Manufacturing Science and Engineering Conference (MSEC 2022). https://doi.org/10.1115/MSEC2022-84991. West Lafayette, USA.
Zheng, B., Wang, H., Huang, Z., Zhang, Y., Zhou, H., Li, D., 2017. Experimental investigation and constitutive modeling of the deformation behavior of Poly-Ether-Ether-Ketone at elevated temperatures. Polym. Test. 63, 349–359.